Characterization of Multiphase Metal Matrix Composites by Means of CT and Neutron Diffraction

Sandra CABEZA, Tatiana MISHUROVA, Giovanni BRUNO
Bundesanstalt für Materialforschung und -prüfung BAM, Berlin, Germany

Contact e-mail: sandra.cabeza@bam.de-

Abstract.
The present study examines the relationship between the microstructure of multiphase metal matrix composites and their damage mechanisms. The matrix AlSi12CuMgNi was combined with 15% vol. Al_2O_3 (short fibers), and with 7% vol. Al_2O_3 + 15% vol. SiC (short fibers and whiskers, respectively). The experimental approach encompasses 3D microstructure characterization by means of computed tomography of samples (a) as-cast, (b) after heat treatment, and (c) after compression tests at room temperature. The volume fraction of different phases, their distribution, their orientation, and the presence of defects and damage are studied.
The influence of the addition of SiC particles on mechanical properties of composite was investigated. Phase-specific load partition analysis for samples with fiber plane parallel to load was performed by using neutron diffraction (ND) during *in-situ* compression. ND results show damage in the Si phase, while Al_2O_3 short fibers carry load without damage until failure. The computed tomography observations confirm the load partition analysis.

1. Introduction

Light metals are of interest mainly in the transport sector, where high mechanical performance and weight-saving are targeted. Metal matrix composites (MMC) represent an improvement of mechanical properties such as modulus, static and fatigue strength, while lowering the average density.
The 3D microstructural characterization of Metal Matrix Composites (MMC) aims to achieve insights on size, distribution and orientation of the different phases -matrix and reinforcements- as well as a more precise global value of their volume fractions compared with 2D metallography. Defects coming from fabrication as well as damage after mechanical testing can also be assessed.
Previous studies of Aluminum and AlSi -MC reinforced with alumina short fibers [1-8] have disclosed the role of the anisotropic and interconnected microstructure of the composite: the eutectic Si phase showed an interpenetrating network for Si contents > 7 wt% [4], forming bridges between Al_2O_3 short fibers [3-4] which were oriented randomly within a plane. Altogether the stiffness of the composite has been shown to increase compared to the unreinforced matrix. The overall interconnected 3D structure leads to the improvement of the creep resistance and to the increase of load bearing capacity [5].

2. Experimental methodology

2.1 Materials

The AlSi12CuMgNi alloy [9-11] reinforced with 15%vol of Al_2O_3 – Saffil short fibers (3-phase composite named Type I) and the same alloy reinforced with 7%vol of Al_2O_3 and 15%vol SiC whiskers (4-phase composite named Type II) were produced by means of squeeze casting [12]. The alloy was cast to infiltrate a mat of planar random oriented fibers (preform). For Type II the preform contained also SiC particles. Cylindrical samples for both computed tomography (CT) and neutron diffraction (ND) were machined with plane random fibers parallel to the longitudinal axis.
Some of the samples were subjected to heat treatment at 500°C for 4h in order to study the evolution of the microstructure in these composites, particularly regarding the interconnectivity of the eutectic Si phase.

2.2 Microstructural and damage characterization

Synchrotron CT measurements were carried out at the *BAMline* (BESSY II, HZB Berlin, Germany). The samples were studied in three conditions: (i) as cast (ii) after thermal treatment at 500°C for 4h and (iii) after compression tests. The samples were machined into cylindrical pins 1.5mm in diameter. A monochromatic energy of 25 keV and a pixel size of 0.44×0.44 μm² were chosen. The reconstruction of 3D volumes from 2D projections was made by filtered back projection and a single-distance phase-contrast correction algorithms using ANKAphase software [13]. For the segmentation of the different phases and for the visualization of the reconstructed volumes AvizoFire [14] was used. Volume fractions of intermetallics and reinforcements were obtained from the average of three randomly selected volumes (352×352×352) μm^3, giving standard deviation as error estimation. For the particular case of eutectic Si, segmentation was difficult due to close grey scale value to the aluminum matrix. Therefore, its volume fraction was obtained by averaging 2 volumes (352x352x352) μm^3 and 3 different grey value thresholds. In order to check the statistical significant of these volumes, also a bigger one (704x704x704) μm^3 with the same 3 thresholds was analyzed and yielded similar values. As for the pre-strained samples from compression tests (see below on 2.2), the volume fractions of cracks were calculated from the average of 3 volumes (440×440×220) μm^3.

2.3 Mechanical characterization

Ex-situ and *in-situ* compression tests were carried out. Cylinders -4mm diameter, 8mm length- with Al_2O_3 fibers plane parallel to the longitudinal axis were compressed *ex-situ* at room temperature and at strain rate of 10^{-4} s^{-1} in a n a universal servo-hydraulic test rig with a load cell of 20kN (CENIM-CSIC, Madrid, Spain).
Neutron diffraction measurements were done during *in-situ* compression at E3 line (BERII, HZB, Berlin, Germany). A monochromatic beam of wavelength λ=1,476 Å and a gauge volume of 6×3×2 mm^3 were used. Cylinders -6 mm diameter, 12 mm length- were tested in two perpendicular orientation (see Fig. 1). The specimens were compressed using the load frame available with a load cell of 50kN, measuring principal strains in axial and radial directions.
The evolution of volume lattice strains with the applied load was determined through the shift of the position of Al-311, Si-422 and SiC-311 peaks (at 2θ=74º, 2θ=83° and 2θ=68°, respectively). The diffraction peaks were fitted with a Gaussian function using the software

StressTexCalculator. The diffraction peak of the alumina short fibers could not be observed due to nanocrystalline structure of the fibers.

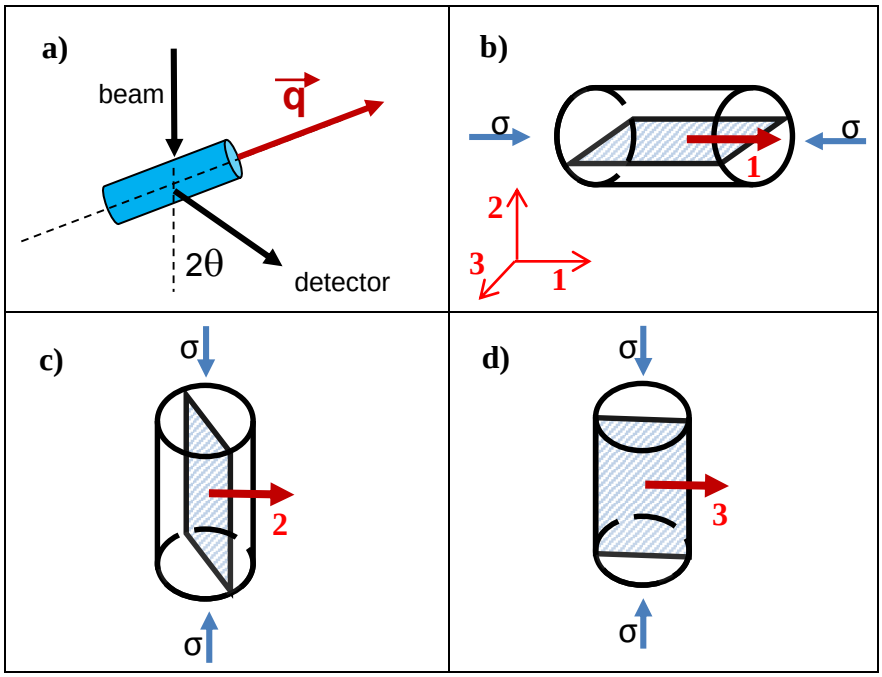

Fig.1. (a) Schematic setup of neutron diffraction experiment (q is scattering vector, θ is scattering angle); (b) axial component; (c) radial out-of-plane component; (d) radial in plane component measurement set-ups.

Since d_0 references (unstrained lattice parameters) were difficult to obtain for each phase of composites, calculation of principal stresses difference (eq.1) was performed:

$$\sigma_1 - \sigma_2 = -\frac{E}{1+\nu}(\theta_1 - \theta_2)\,\mathrm{ctg}\,\theta_0$$
$$\sigma_1 - \sigma_3 = -\frac{E}{1+\nu}(\theta_1 - \theta_3)\,\mathrm{ctg}\,\theta_0 \qquad (1)$$
$$\sigma_2 - \sigma_3 = -\frac{E}{1+\nu}(\theta_2 - \theta_3)\,\mathrm{ctg}\,\theta_0$$

where $\sigma_1, \sigma_2, \sigma_3$ are the principal stresses, which can be calculated from ND measurements (see set-up in Fig.1), E is Young's modulus, ν is Poisson's ratio, θ_1, θ_2, θ_3 are measured Bragg angles along the principal sample directions (1,2,3), and θ_0 is the reference Bragg angle (pre-load).

We used the following peak specific elastic constants: E_Al^{311} = 69,4 GPa, ν_Al^{311} = 0,35 for the aluminum phase and E_Si^{422} = 167,35 GPa and ν_Si^{422} = 0,215 for the silicon phase, E_SiC^{311} = 460 GPa, ν_SiC^{311} = 0,153 for the SiC phase. They were calculated using a Kröner model [15]. The principal stresses differences of Al_2O_3 fibers could be obtained from the global stress balance condition of equation 2:

$$\sigma_{Al2O3} = \frac{\sigma_{app} - (1 - f_{Al2O3} - f_{Si} - f_{SiC})\sigma_{Al} - f_{Si}\sigma_{Si} - f_{SiC}\,\sigma_{SiC}}{f_{Al2O3}} \qquad (2)$$

where σ_{app} is the applied stress, f are the volume fractions, and σ are the previous calculated stresses of each phase. Equation (2) is valid for each stress component (whereby σ^2_{app}=σ^3_{app}=0).

3. Results

3.1 Microstructural characterization

The 3D microstructural characterization of composites in as cast condition by means of synchrotron CT is summarized in Figure 2. From the 2D slices of 3D reconstruction of composite Type I and Type II (Fig.2a, and d, respectively) the phases are identified based on their grey scale as follows: grey as Al matrix, dark grey as eutectic Si, white as intermetallic particles (Fe-, Ni- and Cu-rich) [9], light grey as Al_2O_3 fibers and also SiC whiskers, and black as pores/cracks (air). The ceramic reinforcements – Al_2O_3 and SiC- of Type II (Fig.2d) could be analyzed separately neither by global segmentation (due to their similar grey values), nor based on geometry (due to contact between the two). However, the segmentation of the total ceramic reinforcement proved the orientation of Al_2O_3 fibers randomly within XY plane (Fig.2.b). The SiC was observed to agglomerate (Fig.2d). The intermetallic particles were disconnected and heterogeneous in size and shape for both composites (different colors in Fig.2.c and f). The nature of different intermetallics could not be assessed based only on CT measurements, due to their similar absorption (grey value). The volume fractions on Table 1 proved to be in good agreement with the theoretical composition for both composites: 15 and 22% reinforcement for Type I and II, respectively, and similar Si (~7%vol) and intermetallic (~5%vol) phases. The porosity value was under the detectability of CT reconstruction, proving the good quality of the squeeze casting manufacturing process for this kind of composites. It could be also concluded from Table 1 that the thermal treatment did not have any significant influence on volume fractions.

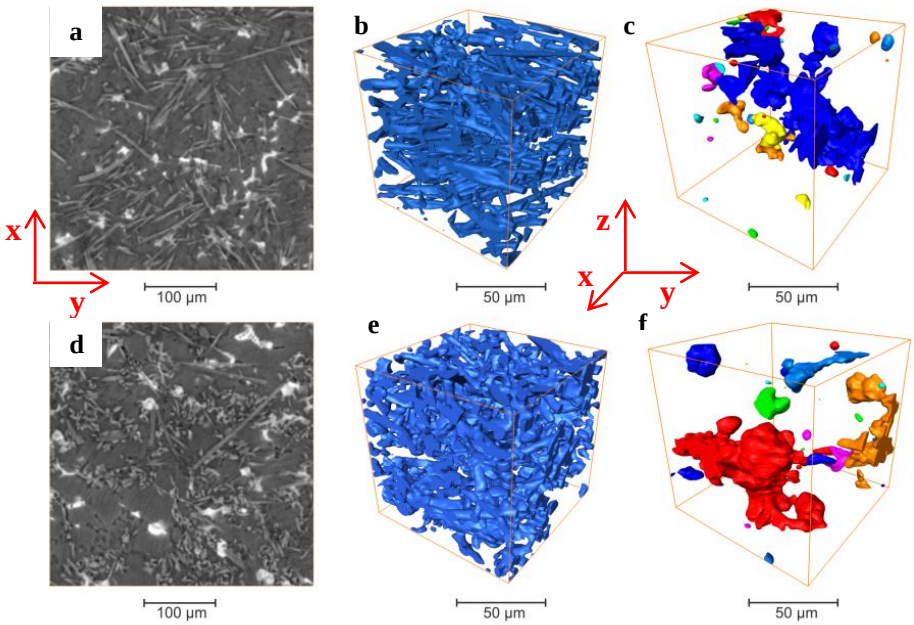

Fig. 2. Micro-CT reconstruction and phase visualization of Type I (a) 2D reconstructed slice, (b) Al2O3 reinforcement, (c) intermetallic particles; Type II (d) 2D reconstructed slice, (e) Al2O3 and SiC reinforcement (f) intermetallic particles.

Table 1. Volume fraction of each phase for studied materials (AC-as cast, TT-thermal treated condition).

Sample	Eutectic Si	Reinforcement	Intermetallics
Type I AC	(7.1±1.5)%	(15.6±0.5)%	(4.9±0.7)%
Type I TT	(6.4±1.2)%	(15.4±0.4)%	(5.2±0.5)%
Type II AC	(7.5±1.6)%	(21.9±0.6)%	(4.6±0.4)%
Type II TT	(6.5±0.9)%	(21.8±0.2)%	(5.4±0.3)%
Nominal	7%	15% (Type I) 22% (Type II)	-

However, the thermal treatment did affect the interconnectivity of the eutectic Si phase (Figure 3). The volumes from Fig.3a,b,d,e disclose Si particles with different colors when disconnected. The histograms (Fig.3c,f) represent the appearance frequency of sizes of an equivalent diameter of Si particles. The distributions for small particles look similar for both composites before and after TT. For Type I (Fig.3c) the big interconnected red Si particle (Fig.3a,b) almost disappears after TT, while for the Type-II (Fig.3f) no significant loss of interconnectivity is observed. This effect could be related with the higher volume fraction of reinforcement in Type II compared to Type I composite (22 vs 15%), which inhibits the diffusion of Si.

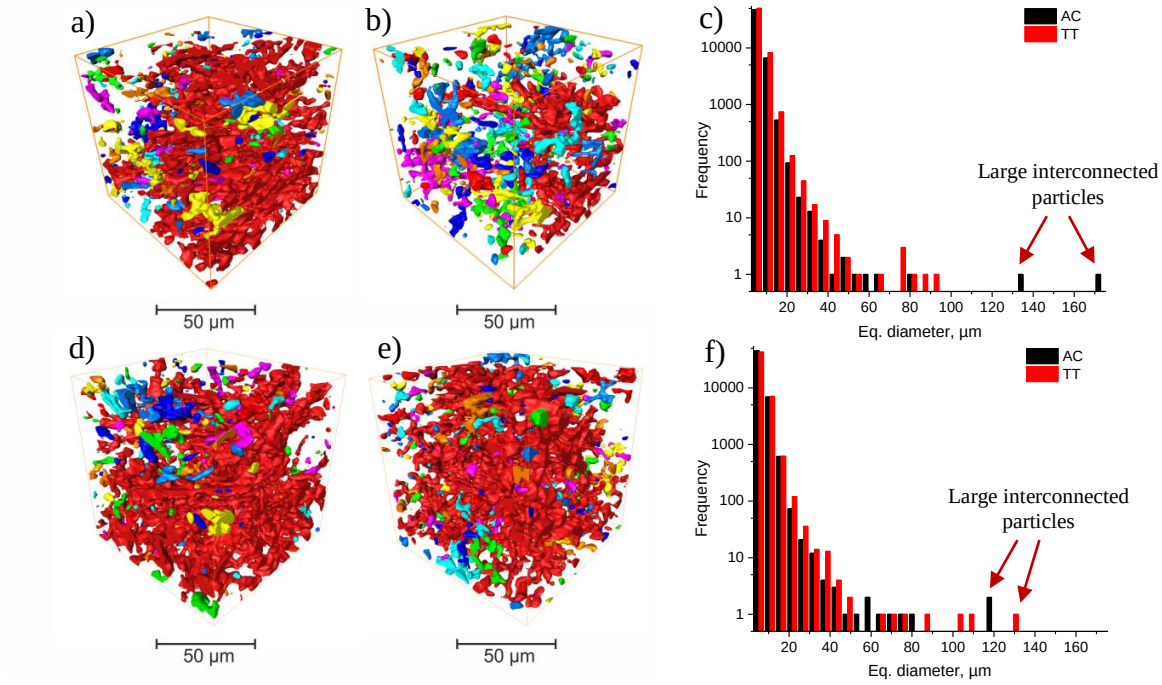

Fig.3. Evolution of eutectic Si phase with thermal treatment (500°C/4h) Type I (a) as cast, (b) after TT, (c) particles size distribution histogram; and Type II (d) as cast, (e) after TT, (f) particles size distribution histogram.

3.2 Load partition characterization

The evolution of phase-specific principal stress differences with applied stress is presented in Figure 4 for the two composites, as well as for the matrix alloy alone as reference. The stress difference $(\sigma_1 - \sigma_2)$ was chosen as the most relevant. Type I sample was tested until failure (Fig.4b), while Type II (Fig.4c) was interrupted at similar applied load -and so the unloaded condition (σ_{app}=0MPa) could be measured (Table 2).
For the matrix alloy AlSi12CuMgNi (Fig.4a) the Al phase starts plastifying already at about σ_{app}=100MPa and shows moderate hardening until 175 MPa, when it starts carrying more load. As for the Si phase, the onset of plastic regime starts later at about 150MPa and presents a sharp increase, meaning that this phase is carrying a higher amount of applied load. However, above σ_{app}=200MPa this tendency is milder, which could imply incipient damage. This scenario would explain the fact that the Al phase carries more load. In this regime for Type I material (Fig.4b), the Al phase behaves in a similar fashion as shown for the matrix alloy, with an extended onset of plastic regime above 200 MPa. Now the Al_2O_3 fibers are carrying most of the load, as reflected by the sharp increase in the slope (hardening). The Si phase starts plastifying at 200MPa for both composites and presents damage above 450 and 400 MPa for Type I and II, respectively, when the Al_2O_3 fibers start carrying more load. The stress on SiC phase (Fig.4c) follows the same tendency as the Si phase and seems to suffer damage slightly above 400MPa to later minimally increase. SiC carries also little more load when Si phase shows damage. The stress differences $(\sigma_1 - \sigma_2)$ and $(\sigma_1 - \sigma_3)$ for each composite show similar results.
It is interesting to note (Table 2) that residual stresses invert their sign after unloading for Si and Al phases, while it becomes strongly compressive for Al_2O_3.

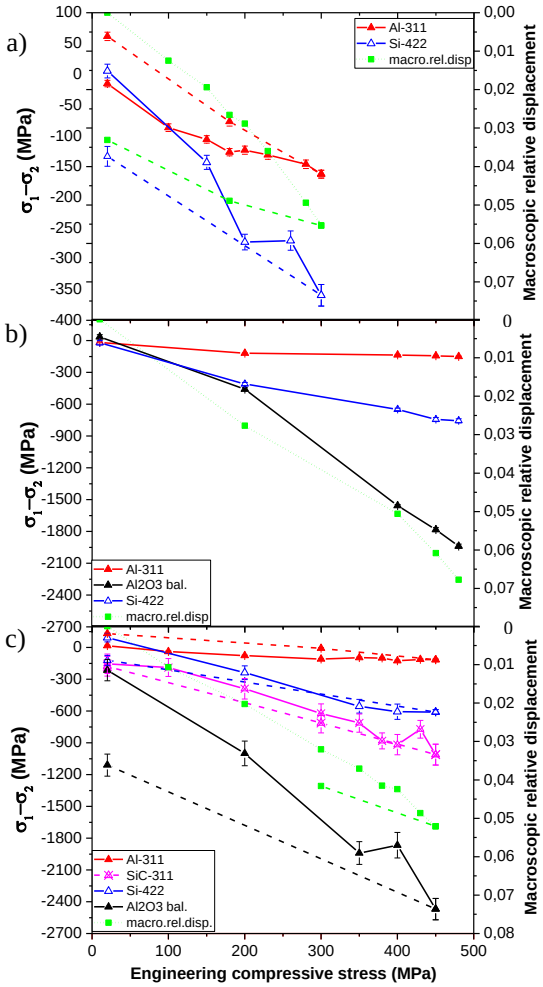

Fig.4. Principal stress difference (σ_1-σ_2) as function of applied stress for (a) matrix, (b) Type I and (c) Type II.

Table 2. Principal stress difference (σ_1-σ_2) retained residual stress (unloading condition) for each phase on matrix and Type II from Figure 4 (in MPa).

Sample	Al	Si	SiC	Al2O3 bal.
Matrix	61	-134	-	-
Type II	130	-122	-178	-1110

3.3 Damage characterization

Mechanical properties from compression tests are given in Table 3. Type I composite presents the highest mechanical strength in compression, due to its higher fraction of Al_2O_3 fibers in axial (loading) direction. The onset of plasticity (yield strength) is also remarkably then Type II.

Table 3. Mechanical properties from ex-situ compression tests at RT and $10^{-4}s^{-1}$ with related volume fraction of cracks from ex-situ CT analysis (Fig.5) – YS yield strength UTS ultimate tensile strength, ε strain.

Sample	YS (MPa)	UTS (MPa)	ε %	%vol.cracks
Matrix	-	-	5,5 (interrupted)	1,2±0,1%
Type I	445	517	4,7 (failure)	0,3±0,1%
Type II	400	447	4,1 (failure)	2,3±0,2%

Figure 5 shows the CT analysis of *ex-situ* compressed samples. The 2D-slices of 3D reconstructions present damage in the form of black cracks. As pointed by red arrows in Fig.5a, in the matrix alloy the damage of eutectic Si phase is clearly observed, as well as some sporadic cracks in intermetallics (in white). In comparison, the composites showed no damage in intermetallics. Furthermore the ceramic reinforcements –both Al_2O_3 and SiC- do not break (Fig.5b,c). Some debonding at the interfaces of SiC with the matrix could be observed (arrow on Fig.5c). Although not disclosed by CT, debonding between Al_2O_3 and matrix cannot be excluded. For composites, damage is present within the Si phase, even progressing into Al matrix for Type II. The 3D rendering of Fig.5d-f gives disconnected cracks, their volume fractions are presented in Table 3. Although the two composites present similar strains to failure, the addition of SiC favored higher volume of cracks in Type II composite.

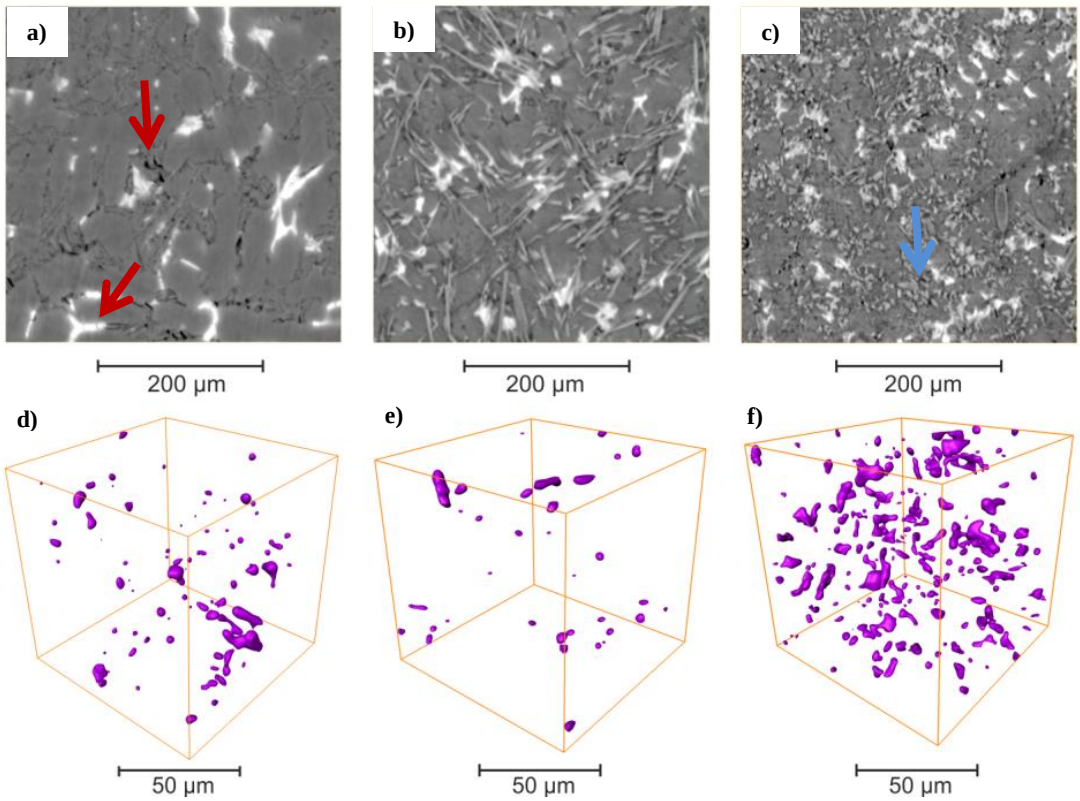

Fig.5. 2D slices from the reconstructed 3D volume from micro-CT measurements after compression for (a) matrix alloy until 7% strain, (b) type I parallel until failure, (c) type II parallel until failure; and 3D rendering of cracks for (d) matrix (1,2%), (e) type I parallel until failure with (0,3%) and (f) type II parallel until failure (2,3%).

4. Discussion and Conclusions

The 3D microstructure characterization proved good correlation with theoretical volume fractions for each phase. However, absorption tomography alone could not differentiate phases with close absorption coefficients such as Al_2O_3 and SiC, and intermetallic particles. The combined addition of Al_2O_3 short fibers and SiC whiskers to the AlSi12CuMgNi matrix alloy significantly influences the thermal and mechanical behavior of the material. On the one hand, the 4-phase composite is more insensitive to thermal treatment as observed for the interconnection of Si phase (Fig.3). On the other hand, although the mechanical strength decreased slightly (due to the minor change on Al_2O_3 content from 15% –Type I- to 7% -Type II), Type II material shows a higher volume of damage for similar compression strain (Table 3). The addition of SiC should therefore promote higher toughness of the material.
The CT observations confirm the *in-situ* load partition tendencies (Fig.4): the Si phase fails and Al_2O_3 fibers -oriented parallel to the load -carry most of the load but do not break. Furthermore, the partial debonding observed at the SiC interface with the matrix (blue arrow-Fig.3c) explains the minimal damage of this phase during *in-situ* experiments. However, the slight increase above σ_{app}=400 MPa indicates that the SiC phase is still effectively reinforcing.
The plastic deformation of MMC reinforced with short fibers is strongly affected by two competing mechanisms [6,7,16-18]: (i) The load transfer from the soft matrix to the stiff short fibers; (ii) The internal damage, reducing the load-bearing capacity of the fibers in the form of fiber fragmentation, buckling and debonding.
Load partition behavior in compression for both composites (Fig.4) can be rationalized in three different behaviors: 1- *elastic* (until 200MPa), 2- *matrix strain hardening* or matrix plasticity (until 400 and 350MPa for Type I and II, respectively), and 3- *damage* (until failure). These regions have been reported in previous studies on composites with both Al and Al-Si matrices [6,7,10]. The AlSi12CuMgNi as matrix alloy for composites shows an improvement of some mechanical properties with respect to formerly studied matrices, which is related to the presence of the 3D networks formed by eutectic Si and intermetallic particles. In fact, an onset of the Al plastic regime from 60 MPa (in the case of pure Al matrix [7]) and 100 MPa (AlSi12 [6]) to about 200 MPa for AlSi12NiCuMg is observed (Fig.4b,c). Furthermore, failure occurred at about 205 MPa and 320 MPa for Al and AlSi12 matrix composites with similar reinforcement, respectively, while for AlSi12NiCuMg composites the stress to failure increased above 450 MPa.
Damage does appear in the form of cracks within the eutectic Si and the intermetallic phases for matrix (Fig.5a,d). However, Type I presented little damage-a few cavities in eutectic Si-hence it is assumed that failure occurs as the propagation of a single crack. Since no debonding between Al_2O_3 fibers and matrix interfaces is resolved, short fibers can still be considered as reinforcing phases during loading until failure (Fig.4b,c). In contrast, in Type II composite the SiC phase did not present damage but sporadic opening of cracks at the interface with the matrix (Fig.5c), losing part of their ability to bear load above 400MPa (Fig 4c).

References

[1] V.S. Zolotorevsky, N.A. Belov, M.V. Glazoff, Casting Aluminum Alloys, Elsevier, New York, 2007.

[2] G. Garcés, G. Bruno, A. Wanner, Scripta Materialia 55 (2006) 163-166.

[3] G. Requena, G. Garcés, Z. Asghar, E. Marks, P. Staron, P. Cloetens, Adv Eng Mat 13 (2010) 674-684.

[4] F. Lasagni, H. P. Degischer, J of comp mat 1 (2009) 739-755.

[5] G. Requena, P. Degischer, E. Marks, E. Boller, Mat Sci and Eng A, 487 (2008) 99–107.

[6] G. Requena, G. Garcés, S. Danko, T. Pirling, E. Boller, Acta Mater 57 (2009) 3199-3212.

[7] G. Garcés, G. Bruno, A. Wanner, Acta Mater 55 (2007) 5389-5400.

[8] G. Garces, G. Bruno, A. Wanner, Mat Sci and Eng A 417 (2006) 73–81.

[9] Z. Asghar, G. Requena, E. Boller, Acta Mater 59 (2011), 6420-6432.

[10] Z. Asghar, G. Requena, Mat Sci and Eng A 591 (2014) 136-143.

[11] G. Requena, H.P. Degischer, Mat Sci and Eng A 420 (2006) 265–275.

[12] D. B. Miracle, S. L. Donaldson, ASM Handbook, vol. 21, Composites, 2001. ISBN: 978-0-87170-703-1.

[13] T. Weitkamp, D. Haas, D. Wegrzynek, A. Rack, J of Sync Rad 18 (2011) 617-629.

[14] AvizoFire ⟨http://www.vsg3d.com/⟩.

[15] H. Behnken, V. Hauk: Z. Metallkde. 77 (1986), 620-626 (in German).

[16] T. L. Dragone, J.J. Schlautmann, W.D. Nix, Metal Trans A 22 (1991) 1029.

[17] A. Doughly, N. Merk, G. Eggeler, Acta Metal Mater 43 (1995) 535.

[18] A. Doughly, N. Merk, G. Eggeler, Acta Metal Mater 41 (1993) 3245.